A metabolic prosurvival role for *PML* in breast cancer

Arkaitz Carracedo,[1,2] Dror Weiss,[1] Amy K. Leliaert,[3] Manoj Bhasin,[4] Vincent C.J. de Boer,[5] Gaelle Laurent,[5] Andrew C. Adams,[6] Maria Sundvall,[1] Su Jung Song,[1] Keisuke Ito,[1] Lydia S. Finley,[5] Ainara Egia,[1] Towia Libermann,[4] Zachary Gerhart-Hines,[7] Pere Puigserver,[7] Marcia C. Haigis,[5] Elefteria Maratos-Flier,[6] Andrea L. Richardson,[8] Zachary T. Schafer,[3] and Pier P. Pandolfi[1]

[1]Cancer Genetics Program, Beth Israel Deaconess Cancer Center, Departments of Medicine and Pathology, Beth Israel Deaconess Medical Center, Harvard Medical School, Boston, Massachusetts, USA. [2]CIC bioGUNE and IKERBASQUE, Basque Foundation for Science, Bizkaia, Spain,. [3]Department of Biological Sciences, University of Notre Dame, Notre Dame, Indiana, USA. [4]Division of Interdisciplinary Medicine and Biotechnology, Beth Israel Deaconess Medical Center, and [5]The Paul F. Glenn Labs for the Biological Mechanisms of Aging, Department of Pathology, Harvard Medical School, Boston, Massachusetts, USA. [6]Departments of Medicine and Endocrinology, Beth Israel Deaconess Medical Center, Boston, Massachusetts, USA. [7]Department of Cancer Biology, Dana-Farber Cancer Institute, Harvard Medical School, Boston, Massachusetts, USA. [8]Department of Pathology, Brigham and Women's Hospital, Boston, Massachusetts, USA.

Cancer cells exhibit an aberrant metabolism that facilitates more efficient production of biomass and hence tumor growth and progression. However, the genetic cues modulating this metabolic switch remain largely undetermined. We identified a metabolic function for the promyelocytic leukemia (*PML*) gene, uncovering an unexpected role for this bona fide tumor suppressor in breast cancer cell survival. We found that *PML* acted as both a negative regulator of PPARγ coactivator 1A (PGC1A) acetylation and a potent activator of PPAR signaling and fatty acid oxidation. We further showed that *PML* promoted ATP production and inhibited anoikis. Importantly, *PML* expression allowed luminal filling in 3D basement membrane breast culture models, an effect that was reverted by the pharmacological inhibition of fatty acid oxidation. Additionally, immunohistochemical analysis of breast cancer biopsies revealed that PML was overexpressed in a subset of breast cancers and enriched in triple-negative cases. Indeed, *PML* expression in breast cancer correlated strikingly with reduced time to recurrence, a gene signature of poor prognosis, and activated PPAR signaling. These findings have important therapeutic implications, as *PML* and its key role in fatty acid oxidation metabolism are amenable to pharmacological suppression, a potential future mode of cancer prevention and treatment.

Introduction

It is well established that reprogramming of cellular metabolism by cancer genes is a key step in cancer pathogenesis and progression (1). Indeed, more than a century ago, Otto Warburg demonstrated that cancer cells exhibit aberrant metabolic features; the preference of cancer cells for metabolizing glucose inefficiently through anaerobic glycolysis, rather than via the tricarboxylic acid cycle, was therefore termed the Warburg effect (1). In recent years, the concepts outlined by Warburg have been revisited from a molecular perspective (2, 3). As a result, we now have a better understanding of how and why cancer cells attain their metabolic reprogramming (4). It has become apparent that both oncogenes and tumor suppressor genes help maintain the physiological metabolic homeostasis of the cell while it is functional. In contrast, their deregulated activities often trigger a metabolic switch with features similar to those originally described by Warburg. Within this conceptual framework, major tumor suppressor genes have been found to act as central regulators of cellular metabolism (1).

The promyelocytic leukemia (*PML*) gene negatively regulates survival and proliferation pathways in cancer, functions that have established it as a classical proapoptotic and growth inhibitory tumor suppressor (5). PML is the essential component of multi-protein subnuclear structures commonly referred to as the PML–nuclear bodies (PML-NB, ref. 6), in which PML multimerizes to function as a critical scaffold for the composition and assembly of the entire complex, a process that is regulated by small ubiquitin-like modifier–mediated (SUMO-mediated) modifications and interactions (7, 8). PML likewise regulates a wide variety of biological processes (9). Despite the established role of PML and PML-NBs in solid tumors and leukemia pathogenesis, little is known about the role of this tumor suppressor in the regulation of cancer metabolism.

Our knowledge of the contribution of fatty acid oxidation (FAO) to cancer initiation and progression is also limited to a handful of recent studies (10–12). We know that in breast cancer cells, FAO functions as the source of ATP when epithelial glandular structures lose their normal architecture and cancer cells start to proliferate aberrantly, migrating far from the extracellular matrix and hence undergoing metabolic stress (10). This loss of attachment results in the inhibition of glucose uptake and glycolytic influx, and the ensuing decrease in redox power (NADPH) leads to increased reactive oxygen species, which inhibits fatty acid catabolism. Importantly, restoring FAO by means of antioxidant treatment increases the survival capacity of these cells upon loss of attachment. On the other hand, in leukemia cells, FAO provides a survival advantage in an ATP-independent manner, possibly through the expression of uncoupling protein 2 (UCP2) (11, 13). Indeed, pharmacological inhibitors of FAO have been suggested as potential anti-leukemic compounds.

Authorship note: Dror Weiss, Amy K. Leliaert, and Manoj Bhasin contributed equally to this work.

Conflict of interest: The authors have declared that no conflict of interest exists.

Citation for this article: *J Clin Invest.* doi:10.1172/JCI62129.

In this study, we demonstrate that PML regulates PPARγ coactivator 1A (PGC1A) acetylation and PPAR signaling and that its presence provides a selective advantage in breast cancer, thus identifying this tumor suppressor as an unexpected promoter of tumoral metabolic reprogramming.

Results

PML opposes a metabolic syndrome in vivo by favoring fatty acid catabolism. While evaluating the role of PML in cellular metabolism, we have unexpectedly unraveled a function for this tumor suppressor in the catabolism of fatty acids. Loss of *Pml* resulted in decreased FAO in both primary and transformed mouse embryonic fibroblasts (MEFs) (Figure 1A and Supplemental Figure 1A; supplemental material available online with this article; doi:10.1172/JCI62129DS1) as well as in primary hepatocytes (Figure 1B), in which we discovered a 30%–40% decrease in active FAO corrected by blank counts (in etomoxir-treated conditions). Conversely, overexpression of PML elevated this metabolic pathway in HepG2 hepatoma cells (50% increase in active FAO corrected by blank counts; Figure 1C). Similar results were observed in HEK293 cells (data not shown). In addition, a dose of arsenic trioxide (ATO), which promotes PML degradation (14, 15) and does not induce apoptosis or loss of mitochondrial membrane potential (16, 17), significantly reduced dehydrogenation of ^{3}H palmitate (readout of FAO), by 20%, in line with the downregulation in PML protein levels (Figure 1D).

Alterations in FAO have been associated with obesity in rodents (18–21). Moreover, genetic or pharmacological modulation of regulators of FAO, such as Sirt1 or PPARs, have an impact on diet-induced obesity (22–25). Therefore, we evaluated whether loss of *Pml* would result in an increased predisposition to obesity.

We first studied the consequences of subjecting adult *Pml* WT and KO mice of a pure 129Sv genetic background to a high-fat diet (HFD) (60% of calories from fat) or to a control diet (LFD) (10% calories from fat) for 20 weeks. In line with our hypothesis, HFD-fed *Pml*-deficient mice exhibited a significant increase in body weight and fat mass compared with WT mice (Figure 1, E–G and ref. 26). Importantly, the augmented sensitivity to HFD-induced obesity was associated with parameters of metabolic syndrome, including exacerbated glucose intolerance and serum leptin levels (Figure 1, H and I). Notably, the activity and food intake of *Pml* WT and KO mice were indistinguishable in both diet regimes (Supplemental Figure 1, B and C), suggesting that the observed obesity predisposition arises at least in part as a consequence of an intrinsic metabolic alteration in fatty acid catabolism, in line with previous reports (24, 25).

To further evaluate whether Pml could play a role in metabolic adaptation in vivo, we employed a genetic mouse model of obesity based on the inactivating mutation of the *Leptin* gene. *Leptin* homozygous mutants exhibit early onset obesity, together with signs of metabolic syndrome and other features, such as sterility (27). *Leptin* deficiency results, among other things, in hyperphagy due to alterations in satiety mechanisms (27). First, we evaluated the status of *Pml* in $Lep^{Ob/Ob}$ mice. A fraction of hepatocytes in these mice exhibited a marked upregulation of *Pml*, as assessed by immunohistochemical analysis. $Lep^{Ob/Ob}$ hepatocytes displayed prominent Pml-NB with a ring shape, similar to those previously reported (ref. 8 and Supplemental Figure 1D). This in turn suggested that Pml could be acting as a response mechanism toward metabolic adaptation in $Lep^{Ob/Ob}$ obese mice. We therefore hypothesized that loss of *Pml* could exacerbate obesity in $Lep^{Ob/Ob}$ mutants. To explore this thesis, we backcrossed *Pml* mutant mice for 3 generations with C57BL/6 mice and then intercrossed these with $Lep^{Ob/Ob}$ mice (pure C57BL/6) for 3 generations to generate *Pml*-$Lep^{Ob/Ob}$ double-mutant mice (*Pml* WT-$Lep^{Ob/Ob}$ or Ob-WT and *Pml* KO-$Lep^{Ob/Ob}$ or Ob-KO). Indeed, combined *Pml* and *Leptin* inactivation resulted in a marked increase in obesity and fat mass in compound mutant mice, measured at 2 and 3 months of age, in both males and females (Figure 1J and Supplemental Figure 1, E–J). These results demonstrate that in regulating FAO, Pml plays an important role relevant to organismal physiology.

PML regulates PGC1A acetylation and PPAR transcriptional activity. Next, we aimed to decipher the molecular mechanism involved in the regulation of FAO downstream of PML. To this end, we performed whole-genome gene expression analysis of liver extracts (tissue in which FAO is exquisitely regulated, refs. 28, 29) from *Pml* WT and KO mice. After preprocessing and normalization of data, we identified 127 differentially expressed genes using a random variance *t* test ($P = 0.05$; Supplemental Table 1, real-time PCR validation of genes significantly modulated in the microarray analysis in Supplemental Figure 2A). Interestingly, gene ontology–based (GO-based) enrichment analysis of differentially expressed genes in *Pml*-WT and -KO liver extracts identified a significant overrepresentation of genes related to lipid metabolism ($P = 1.29 \times 10^{-5}$; Figure 2, A and B). FAO is a tightly regulated metabolic process, which is under strict transcriptional control (29). Surprisingly, promoter analysis of genes related to lipid metabolism modulated in *Pml*-KO (Figure 2, A and B) revealed a significant enrichment of peroxisome proliferator–activated receptor-response element–containing (PPRE-containing) genes (0.27 sites per Kb, $P = 0.006$; Supplemental Table 2), in line with the notion that PPAR complexes play a critical role in the regulation of FAO (30, 31).

In order to further study the existence of PPAR signaling alteration in *Pml*-KO mice, we took advantage of publicly available gene expression data (GEO GSE8295) (32). In the referred study, *Ppara*-WT and -KO mice were treated with a PPARA agonist, Wy-14643, to define the genes that are under transcriptional control of this nuclear receptor (32). We first compared the transcripts differentially expressed between *Pml*-WT and -KO with those found in *Ppara*-WT vs. -KO. To this end, we generated a Venn diagram and found 37 coregulated genes (29% of the genes differentially expressed in *Pml*-WT vs. -KO, Fisher's exact test, $P = 3.3 \times 10^{-16}$; Figure 2C). The coregulated genes are depicted in Figure 2D, where the status of these genes in the *Pml*-KO liver is indicated (gene expression validation in Supplemental Figure 2A). Furthermore, a Gene Set Enrichment Analysis (GSEA) identified a significant enrichment of *Pml*-KO downregulated genes (Figure 2E) in the *Ppara*-KO vs. -WT downregulated gene set.

Next, we validated in vitro the effect of PML presence or absence in PPAR function. On the one hand, we evaluated the effect of PML on the activity of PPARs by using a well-established PPAR target, PDK4 (33, 34). In line with our observations, the induction of *Pdk4* upon exposure to palmitate and carnitine (conditions in which the FAO assay is performed) was significantly diminished in primary and transformed *Pml*-KO MEFs (Figure 3A and Supplemental Figure 2B). Importantly, both PPARA and PPARD selective agonists (Wy-14643 and L165-041, respectively) showed reduced *Pdk4*-inducing efficiency in *Pml*-KO MEFs (Figure 3A). On the other hand, we evaluated the effect of PML on PPAR transcrip-

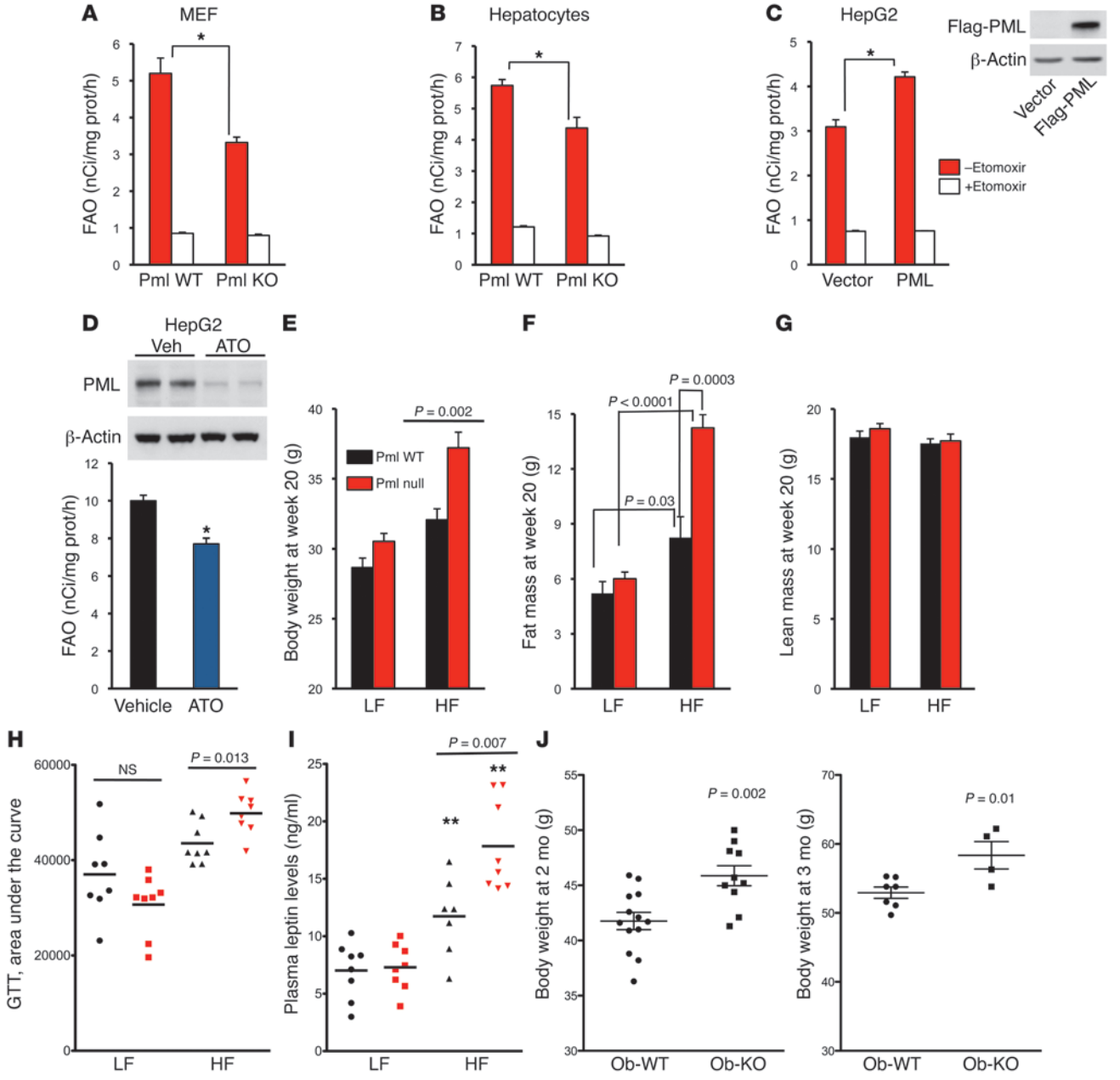

Figure 1

PML regulates FAO and predisposition to obesity. (**A**–**C**) FAO levels in *Pml*-WT and -KO primary MEFs (**A**, $n = 3$) and primary hepatocytes (**B**, 4–5 independent hepatocyte cultures) and in HepG2 cells acutely infected with an empty or a PML-expressing retrovirus (**C**, from 2 independent infections; FAO was measured in triplicate for each infection. Representative Western blot for PML overexpression is shown). Etomoxir 100 μM. Representative experiments are shown. (**D**) FAO levels in HepG2 cells treated with vehicle or ATO (1 μM) for 72 hours ($n = 4$, a representative experiment is shown, right panel indicates PML levels [anti-PML] by Western blot using β-actin as endogenous control). (**E**–**I**) Body weight (**E**), fat mass (**F**), lean mass (**G**), GTT (**H**), and serum leptin levels (**I**) in *Pml*-WT (black bars/symbols) and *Pml*-KO (red bars/symbols) mice subjected to a control (LF) or HFD (HF) ($n = 8$). (**J**) Body weight in *Pml*-WT and *Pml*-KO *Lep*$^{Ob/Ob}$ female mice of the indicated age. *$P < 0.05$. Error bars in **A**–**D** represent mean ± SD; error bars in **E**–**G** represent mean ± SEM.

tional activity by luciferase reporter assays, which indicated that PML modulates PPAR nuclear receptor transcriptional activity (Figure 3B and Supplemental Figure 2C).

PML is the essential component of the PML-NB (7), which host more than 70 proteins and regulate a variety of protein post-translational modification processes, including ubiquitination, SUMOylation, and acetylation (5, 9, 35). A transcriptional cofactor, PGC1A, plays a critical role in the regulation of FAO (36, 37). Interestingly, PML promotes the activity of PGC1A regulators, such as SIRT1, from the PML-NBs (35). PGC1A, when activated, promotes FAO transcriptional program as part of the PPAR complex (24, 37–41). Immunofluorescence and confocal imaging

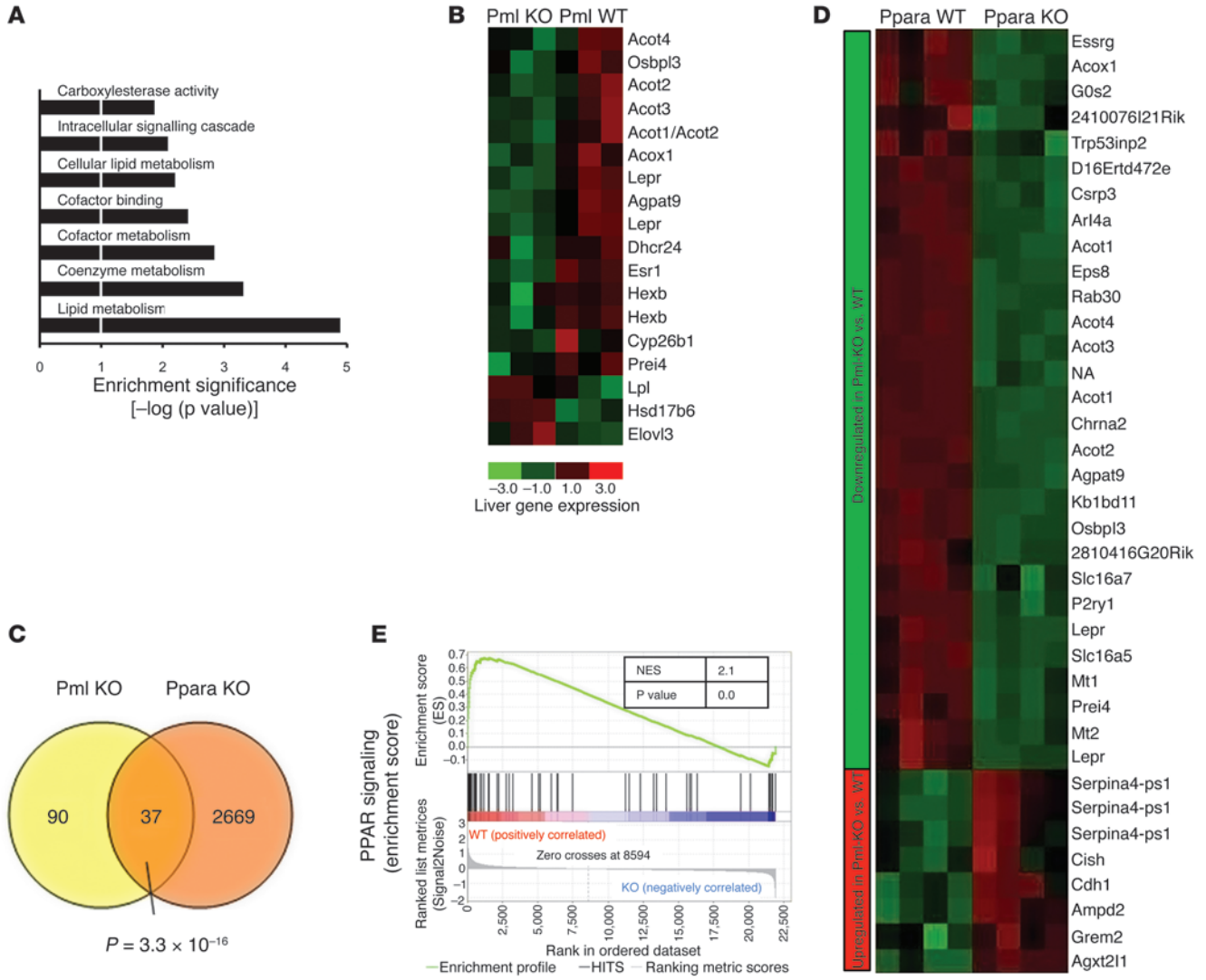

Figure 2

PML loss is associated with defects in PPAR signaling and lipid metabolism. (**A**) GO processes differentially affected in microarray analysis from *Pml*-WT and -KO liver extracts (n = 3). (**B**) Heat map depicting genes related to lipid metabolism from **A** differentially modulated in *Pml*-WT and -KO liver extracts. (**C**–**E**) Venn diagram (**C**), heat map depicting genes differentially expressed (**D**), and GSEA (**E**; the enrichment is depicted by nominal P value and NES) in *Pml*-WT and -KO (**A** and **B**) and in *Ppara*-WT and -KO (see Methods) liver extract microarray that are found coregulated. P value in **C** indicates significance by Fisher's exact test. Green and red colors in **D** represent downregulated and upregulated genes, respectively, whereas the left lateral bar depicts the status of these genes in *Pml*-KO vs. -WT liver extract microarray (green, downregulated in *Pml*-KO; red, upregulated in *Pml*-KO).

revealed that a fraction of PGC1A resides in the PML-NB (Supplemental Figure 2, D–F). PGC1A is localized to the nucleus and shows a diffuse and microspeckled pattern; however, coexpression of its acetyltransferase, GCN5, has been shown to relocalize PGC1A to as yet unidentified subnuclear structures (42, 43). Strikingly, triple immunofluorescence and confocal microscopy imaging revealed that upon coexpression of PML, PGC1A, and GCN5, these 3 proteins strongly colocalized (Supplemental Figure 2, D–F) and physically interacted (Supplemental Figure 2G).

We subsequently evaluated the impact of PML on the function of PGC1A. The activity of PGC1A is regulated by GCN5 and SIRT1, which respectively acetylate and deacetylate PGC1A in at least 13 lysine residues (42, 44, 45). Deacetylation of PGC1A results in its activation (42, 44, 45). Notably, expression of PML reduced the acetylated PGC1A fraction in Flag-PGC1A immunoprecipitates (Figure 3C), hence rendering PGC1A active. GCN5 is required for the acetylation of PGC1A, whereas SIRT1 is the major deacetylase of this protein. In order to define the contribution of PML to this regulatory network, we employed a selective SIRT1 pharmacological inhibitor, EX527 (46). SIRT1 inhibition, from 3 hours up to 24 hours, dramatically increased the acetylation levels of PGC1A while in the presence of PML overexpression, this effect was minimal (around 50% effect of PML in the presence of SIRT1 inhibitor; Figure 3D and Supplemental Figure 2H), in line with the fact that we did not observe a robust colocalization among SIRT1, PGC1A, and PML (Supplemental Figure 2I).

Taken together, our data reveal a previously unidentified function of PML at the core of FAO as a player in the regulation of PGC1A acetylation and PPAR signaling activation.

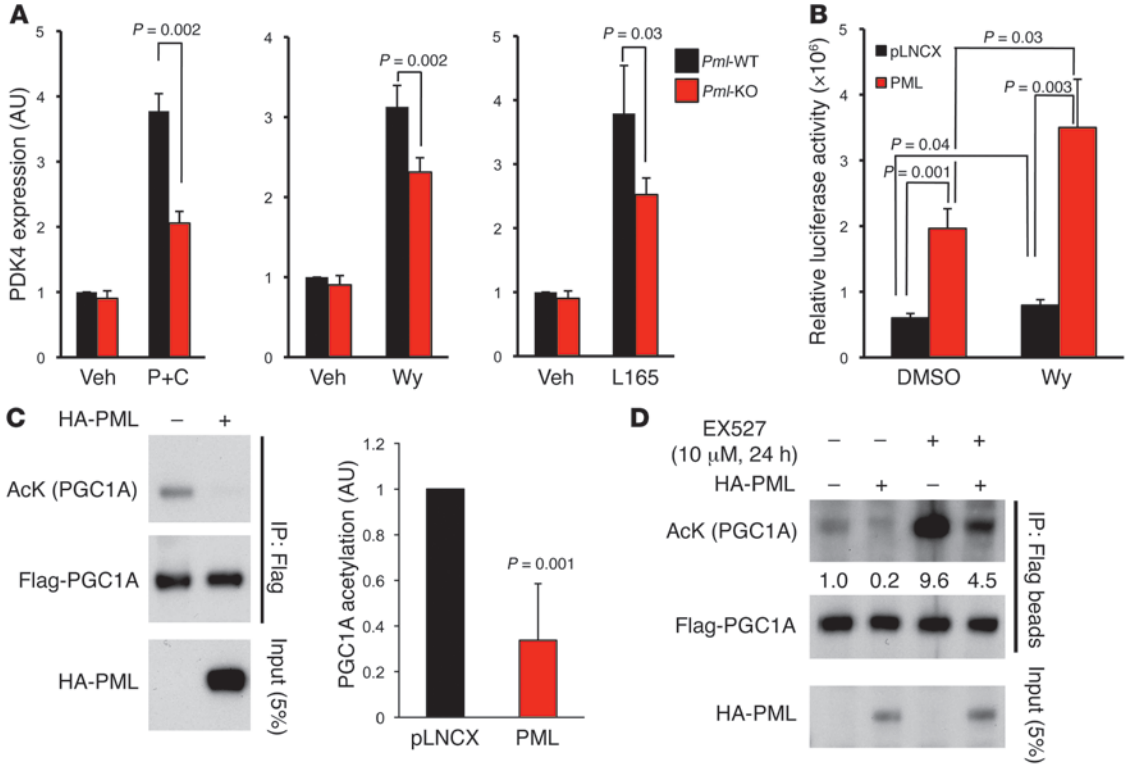

Figure 3

PML regulates PPAR signaling and PGC1A acetylation. (**A**) Real-time PCR analysis of *Pdk4* in transformed (Ras-E1A) MEFs treated overnight with palmitate and carnitine (P+C) (100 μM and 1 mM, respectively, $n = 7$), Wy14643 (100 μM, $n = 3$), and L165041 (10 μM, $n = 4$) using *Glucuronidase B* as endogenous control. Error bars represent mean ± SEM. *P* value indicates statistical significance by *t* test. (**B**) PPAR luciferase reporter activity in HEK293 cells transfected with pLNCX or pLNCX-PMLIV vector upon treatment with vehicle or Wy14643 (50 μM) ($n = 3$). Error bars indicate mean ± SD. (**C**) Western Blot for detection of PGC1A acetylation in PGC1A immunoprecipitates from U2OS cells transfected with empty or PMLIV-expressing vectors ($n = 4$); right panel shows the quantification from 4 independent experiments. Error bars indicate mean ± SD. (**D**) Western blot for detection of PGC1A acetylation in PGC1A immunoprecipitates from U2OS cells transfected with empty or PMLIV-expressing vectors and treated with vehicle or the SIRT1 inhibitor EX527 (10 μM, 24 hours).

PML provides a selective advantage to breast cancer cells undergoing metabolic stress. On the basis of our data, we hypothesized that PML, by promoting FAO, might provide a selective advantage in cancer cells by allowing them to maintain energetic homeostasis when leaving their natural niche. To test this notion, we stably overexpressed PML in a breast epithelial cell line, MCF10A (Figure 4A), which has been previously characterized and used for this type of analysis (10). In line with our results, PML-overexpression increased FAO in detached MCF10A cells (Figure 4B). Moreover, PML overexpression increased ATP levels in conditions of detachment (Figure 4C). Strikingly, increased FAO and ATP production in PML-overexpressing cells correlated with a significant inhibition of anoikis induced by loss of attachment (Figure 4D and Supplemental Figure 3, A and B), suggesting that the metabolic activity of PML in FAO serves as a prosurvival cue in breast cancer cells.

Thus, our data suggest that PPAR signaling and FAO provide a survival advantage to breast cancer cells upon loss of attachment. However, previous data related to the function of PPARA in breast cancer has been controversial. On the one hand, activation of PPARA with Wy14643 reduced the development of malignant mammary tumors in a tumor-prevention setting (47). On the other hand, in human breast cancer–derived cell lines, activation of PPARA promoted proliferation (48). Thus, to define the role of PPARA in conjunction with PML in our experimental model, we carried out loss-of-attachment experiments in breast cancer cell lines that we defined as having high (MDA-MB-231) or low (MCF7) PML levels by Western blot (Supplemental Figure 3C). Pharmacological PPARA inhibition with a commercially available compound (49) decreased cellular viability in both cell lines, whereas high PML-expressing cells were significantly more sensitive (Supplemental Figure 3D). These data suggest that PPARA might have different activities in breast cancer in a context-dependent manner (e.g., tumor-prevention vs. tumor-promotion conditions) and that it is required, at least in part, for cell survival upon loss of attachment.

The proliferation of breast cancer cells into the lumen of hollow glandular structures has been previously modeled in vitro through 3D basement membrane cultures of MCF10A mammary epithelial cells (50). Cells migrating far from the extracellular matrix undergo apoptosis and anoikis in the luminal area of the structure, leading to the formation of glandular hollow structures, whereas promoting FAO prevents this process and leads to luminal filling (10). To determine whether PML would play a role in this process, we grew empty vector or PML-overexpressing MCF10A cells in Matrigel and evaluated apoptosis (Figure 5A) and luminal filling (quantification criteria in Figure 5B). After 10–12 days, the structures arising from empty vector–infected cells exhibited increased apoptosis in the luminal area (Figure 5A). In line with this, the majority of these structures were hollow or mostly clear (Figure 5, B and C). Notably, PML

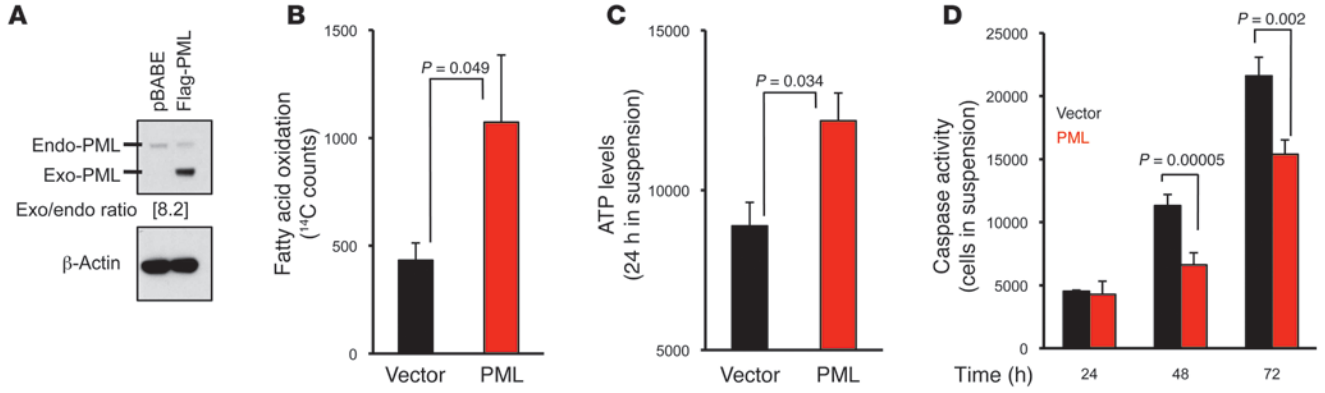

Figure 4
PML expression promotes FAO, ATP production, and cell survival in MCF10A cells. (**A**) Representative Western blot showing Flag-PMLIV expression by anti-Flag antibody in MCF10A cells infected with an empty (pBABE) or PMLIV-expressing (pBABE-Flag-PML) retroviral vector. (**B**–**D**) FAO (24 hours; **B**), ATP levels (**C**), and caspase activity (**D**) at the indicated time points in detached MCF10A cells from **A**.

overexpression in MCF10A cells resulted in decreased apoptosis in the luminal area (Figure 5, A–C) in correlation with an increased percentage of 3D structures exhibiting luminal filling (quantification in Figure 5, B and C). Furthermore, in order to demonstrate that these effects of PML were mediated by its ability to potentiate FAO, we grew PML-expressing MCF10A cells in Matrigel and 8 days later began a treatment with vehicle or etomoxir. As expected, etomoxir completely suppressed the luminal filling induced by PML (Figure 5D and Supplemental Figure 3E). These data provide solid evidence for the proposed selective advantage provided by PML under conditions of loss of attachment, an advantage effected, at least in part, through the activation of the FAO program.

PML is overexpressed in a subset of aggressive breast cancer specimens and correlates with poor prognosis and activated PPAR signaling. Our findings have therefore identified PML as potentially providing a selective advantage to breast cancer cells undergoing metabolic stress. PML was originally identified from the translocation t(15;17) occurring in acute promyelocytic leukemia between this gene and retinoic acid receptor α (*RARA*) (5). Since then, the tumor-suppressive role of PML has been demonstrated in solid tumors, and it has been shown that the PML protein is frequently lost in human cancers (51). However, whether PML expression would be selectively increased in certain settings, providing a selective advantage to tumor cells, is currently unknown.

To test this notion, we evaluated the levels of PML by immunohistochemistry (IHC) in normal breast epithelium as well as in a large set of breast cancer tissues with matched gene expression data (detailed information of the cancers analyzed is shown in Supplemental Table 3). We reviewed the range of staining across normal breast epithelium and tumor samples and developed a semiquantitative scoring scheme as follows: PML 0 = no punctate PML staining in tumor cell nuclei; PML 1+ = single small PML puncta in rare tumor nuclei (~1%–10% with staining); PML 2+ = multiple small to medium PML puncta per nucleus, staining in ~10%–30% of tumor nuclei; PML 3+ = multiple prominent large PML puncta per nucleus, staining in more than 30% of tumor nuclei (Supplemental Figure 4, A and B).

PML immunoreactivity in normal breast epithelial cells was predominantly low or undetectable (0 to 1+ PML staining; Figure 6A and Supplemental Figure 4A). Surprisingly, however, a subset of breast cancers exhibited PML levels in tumor cells that were dramatically higher than those observed in normal epithelium (Figure 6A, representative images of the scoring criteria in Supplemental Figure 4B). We also analyzed whether the high level of PML protein expression observed by IHC correlated with high *PML* mRNA levels. As predicted, we found that there was significant correlation between PML protein and mRNA overexpression only in the tumor cells, but not in the stromal fraction (Supplemental Figure 4C).

We then proceeded to characterize the distinctive features of PML-overexpressing breast cancers. First, we observed a significant direct correlation between PML levels and estrogen/progesterone-negative status (ER/PR negative; χ^2, $P = 0.00002$; Figure 6B). In addition, evaluation of the Bloom-Richardson invasive tumor grade, which is a measure of proliferation and loss of differentiation, revealed a direct relationship between PML expression and a higher grade (χ^2, $P = 0.004$; Figure 6C), suggesting that PML expression is associated with a more aggressive, less differentiated state.

Breast cancers are classified on the basis of their gene expression profiles (52–54). Therefore, we investigated the distribution of tumor subtypes within the different PML expression groups. Notably, the triple-negative breast cancer (TNBC) (ER/PR/HER2 negative, where HER2 is defined as *human epidermal growth factor receptor 2*) or "basal-like" tumors were overrepresented in high (3+) PML–expressing cancers (expected cases 1.6, observed 7, Figure 6D). We further validated these data in 2 additional independent studies, where we could observe a significant upregulation of PML in basal cancers as compared with normal tissue or other subtypes of breast cancer (Supplemental Figure 5).

Tp53 mutation, indicated by aberrant protein accumulation, is observed in a significant fraction of breast cancers and is associated with high tumor grade, negativity for ER receptor, and poor prognosis (55). As reported (56), we found p53 to be upregulated predominantly in basal and HER2 cancers but not in ER (p53 upregulation was observed in 33% of total breast cancer biopsies: 6.6% of ER negative, 44% of HER2, and 73% of basal). Interestingly, PML expression correlated with aberrant expression of p53 protein in this breast cancer cohort (χ^2, $P = 0.002$; Supplemental Figure 6A), which is usually indicative of a p53 mutant state (57). Due to the existence of a small fraction of breast cancers that show upregulation of p53 in the absence of mutation (57) and to

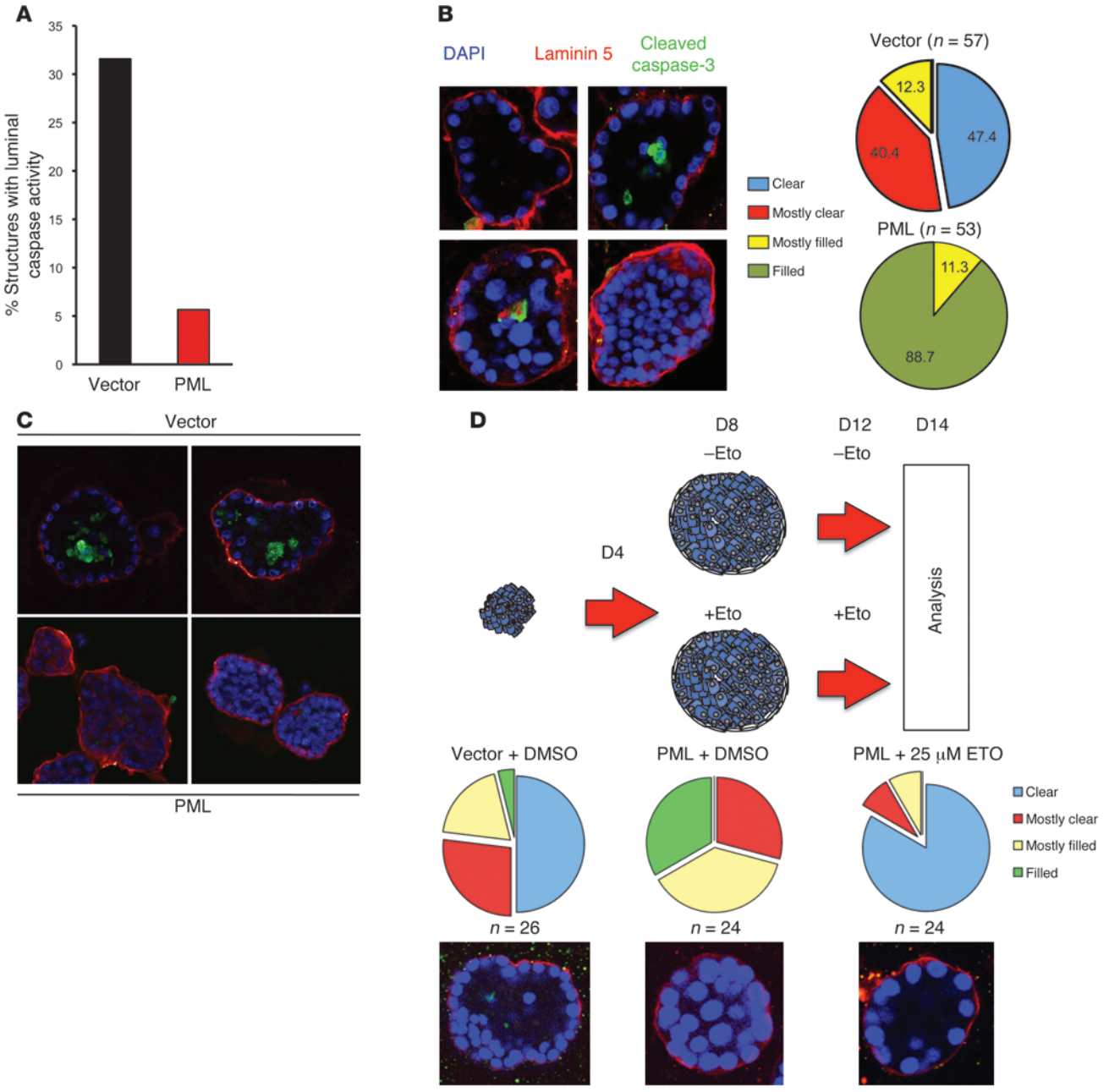

Figure 5

PML expression promotes luminal filling in MCF10A cells in an FAO-dependent manner. (**A**) Caspase-3 positivity in 3D basement cultures of MCF10A cells (day 10 of culture) transduced with an empty or PMLIV-expressing retrovirus. (**B**) Representative fluorescence images (upper panels) used as criteria for quantification of luminal filling of MCF10A cells from Figure 4 (lower panels) cultured in Matrigel for 10 days. (**C**) Representative images of MCF10A cells from Figure 4 cultured in Matrigel for 12 days (as in **B**; from an independent 3D culture). (**D**) Representative scheme of the treatment procedure of MCF10A cells with etomoxir in the 3D model. Lower panels show the quantification of luminal filling after a total of 14 days (6-day treatment with 25 μM etomoxir). *$P < 0.05$; error bars indicate mean ± SD. Original magnification, ×400.

further validate the correlation between p53 mutation and PML upregulation, we analyzed a data set of breast cancer gene expression profiles comprising 251 biopsies, for which p53 mutant status was characterized. In line with our aforementioned results, PML was found to be significantly upregulated in p53 mutant cases (7 out of 10 probes showed significant upregulation; Supplemental Figure 6B), strongly suggesting that PML expression is elevated in breast cancer with inactivated *Tp53*. This is also in full agreement with the observation that PML induction can be supported by aberrant PML protein translation even in the absence of p53 activity (58).

TNBC or basal-like tumors are among the most deadly, undifferentiated, and untreatable breast cancers (59). Since PML overexpression exhibits enrichment for more aggressive types of tumors, we

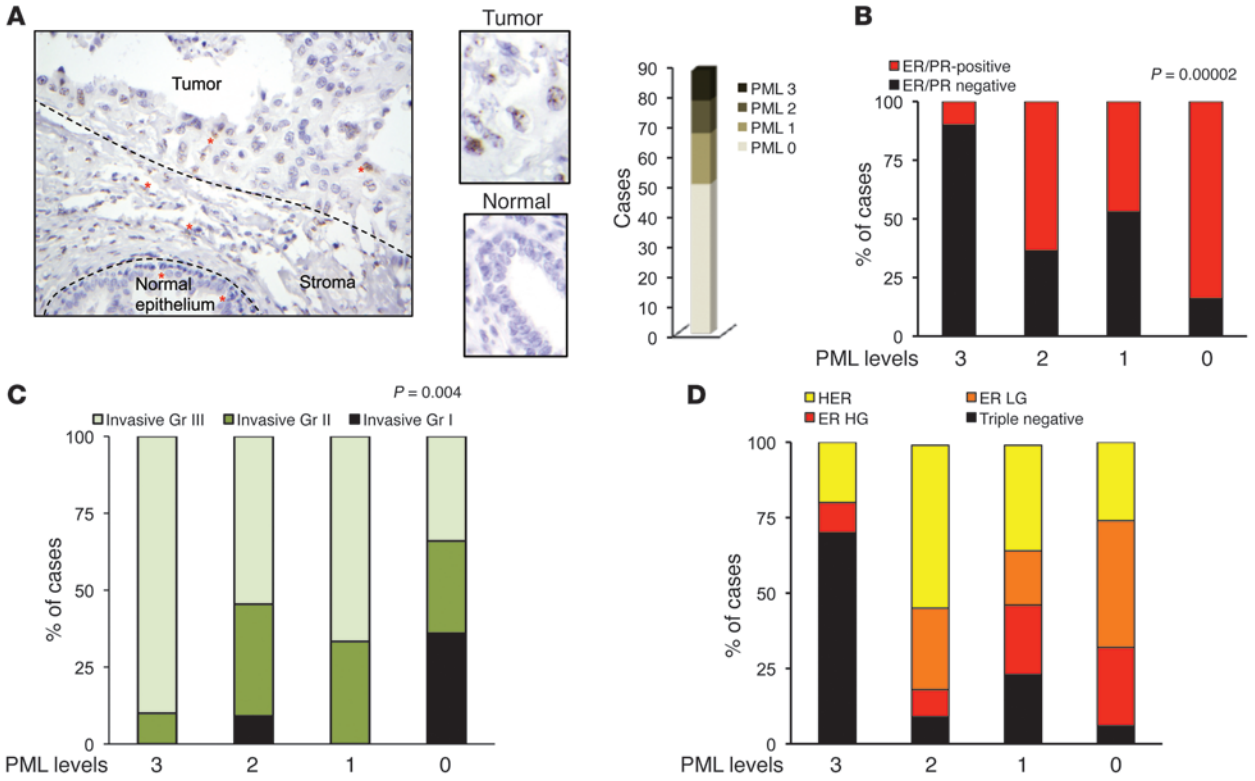

Figure 6

PML is overexpressed in a subset of breast cancers. (**A**) Representative image depicting PML immunoreactivity levels in normal breast epithelium and breast tumor cells (dashed lines delimit the different areas in the field; red asterisks indicate representative PML staining in each cell type). High magnification of a different field from the same slide is shown in central panels. Histogram in right panels shows the number of cases for each group with different PML expression levels by IHC (scoring criteria in Supplemental Figure 4). Original magnification, ×400 (left panel); ×1800 (central panels). (**B**–**D**) Status of ER/PR (**B**), invasive tumor grade (Gr) (**C**), and gene expression subtype (**D**) in the samples analyzed. Modified Scarff-Bloom-Richardson grade scale (82): I, low grade; II, intermediate grade; III, high grade. *P* value reflects χ^2 statistical significance in the correlation analysis. HG, high grade; LG, low grade.

evaluated whether it could serve as a poor-prognosis marker. To this end, we analyzed the time to recurrence of patients whose tumors had been characterized for PML expression. For this analysis, and to discern between a deleterious and an advantageous effect of PML expression in breast cancer, we differentiated between tumors with undetectable (PML 0) and detectable (PML 1+, 2+, 3+) PML expression, which also provided an equilibrated cohort of samples with a substantial number of cases. Interestingly, patients with PML-expressing tumors presented shorter disease-free survival ($P = 0.006$; Figure 7A), which was also observed when comparing the individual score cases (PML 0 vs. PML 1+ vs. PML 2+ vs. PML 3+; data not shown). In order to rule out that PML would bias the analysis of recurrence by being more expressed in TNBC, we next removed the TNBC cases from the analysis. In the 70 cases left upon this adjustment, PML was still significantly associated with shorter disease-free survival (Supplemental Figure 6C). In an effort to define a gene set that would predict for prognosis in breast cancer, van 't Veer et al. performed gene expression profile analyses in a key study that allowed them to establish a signature for poor prognosis (measured by the presence of distant metastasis after 5 years) (60). As expected, GSEA analysis (61) of PML-expressing breast tumors identified significant enrichment in the aforementioned signature for poor prognosis, whereas, conversely, cancers in which PML was undetectable showed a good-prognosis gene expression profile (Figure 7B).

We have shown that PML regulates PGC1A and PPAR signaling to promote FAO, which in turn leads to ATP production and cell survival in breast cancer cells. We therefore tested to determine whether tumors with elevated PML levels would exhibit a signature of increased PPAR activity. Indeed, and strikingly, GSEA analysis in breast tumor samples with detectable vs. not-detectable PML protein levels identified a significant PPAR signaling enrichment (in the top 500 genes downregulated in *Ppara*-KO samples) in PML-expressing tumors (Figure 7C). Eighty-four genes that were downregulated in *Ppara*-KO mice were found upregulated in PML-expressing specimens (Supplemental Figure 7A and validation in Supplemental Figure 7B). Notably, tumors expressing the highest levels of PML exhibited a more profound enrichment in PPAR signature over other classes (Supplemental Figure 7C). Overall, our data show that PML expression is specifically associated with TNBC, high tumor grade, early tumor recurrence, a poor prognosis signature, and a signature of activated PPAR signaling.

Discussion

In this report, we show that PML regulates the activation of the FAO program as well as PGC1A acetylation and the activation of PPAR signaling of unexpected relevance to cancer biology (summarized in Figure 7D). Of note, we find this metabolic network to be of relevance also in modulating the function of hematopoietic stem cells

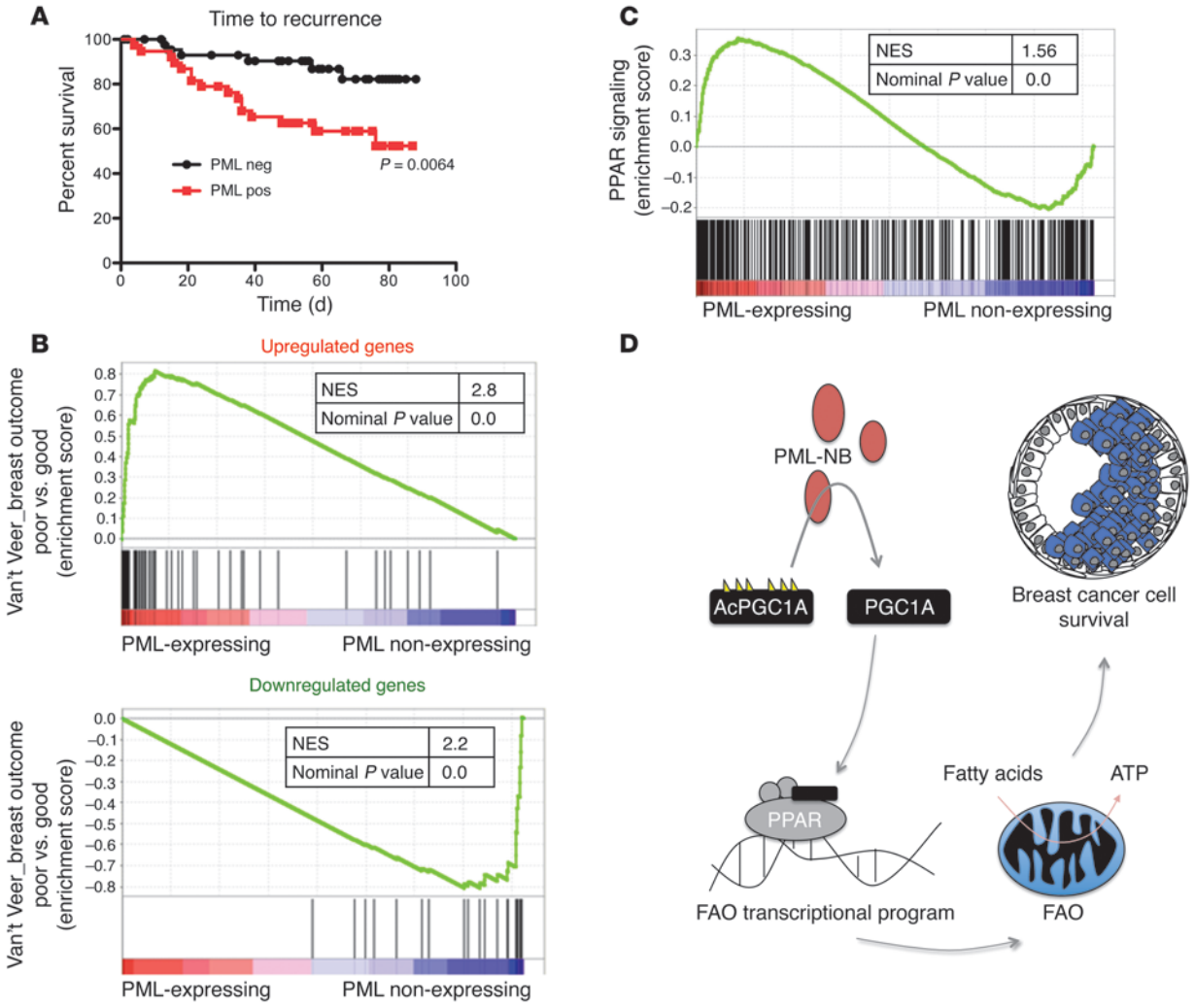

Figure 7

PML overexpression correlates with reduced disease-free survival and poor prognosis in breast cancer. (**A**) Time to recurrence in the group of patients harboring PML-expressing vs. nonexpressing tumors. *P* value indicates the statistical significance by log-rank (Mantel-Cox) test. (**B**) GSEA analysis in PML-expressing vs. nonexpressing tumors shows a significant enrichment in poor-prognosis signature in PML-expressing tumors and a good-prognosis signature in nonexpressing tumors using the signature defined by van 't Veer et al. (60). The enrichment is depicted by nominal *P* value and NES. (**C**) GSEA analysis in PML-expressing vs. nonexpressing tumors shows a significant enrichment in activated *Ppara* signaling (top 500 *Ppara*-KO downregulated genes) in PML-expressing tumors. The enrichment is depicted by nominal *P* value and NES. (**D**) Schematic representation summarizing the main findings in this study. Briefly, PML increases the fraction of deacetylated PGC1A (AcPGC1A and PGC1A represent the acetylated and deacetylated portion of the protein, respectively) and leads to the activation of PPAR signaling and FAO. In turn, FAO increases ATP levels and promotes cell survival and luminal filling in breast cancer, indicating that in these conditions, PML provides a selective advantage in breast cancer.

(62). Interestingly, PML has been shown to regulate the deacetylation and activation of FOXO1 (35), a protein that shares components of the acetylation machinery with PGC1A. Additionally, it has been shown that localization of PGC1A to subnuclear structures upon GCN5 binding allows its interaction with transcriptional cofactors (42, 43). It is therefore plausible that the PML-NB serves as the interface whereby PGC1A interacts with transcriptional components and where its acetylation is dynamically controlled toward activation.

Surprisingly, our data demonstrate that the presence of PML also provides a selective advantage in response to the metabolic stress triggered by conditions of loss of attachment in breast cancer cells. This finding suggests that we revisit the accepted notion that PML serves as a potent proapoptotic factor in all conditions and calls in turn for a more careful analysis of the environmental and genetic milieu in which the presence of PML might provide a selective advantage rather than a clear disadvantage (63). While PML is tumor suppressive in most of the settings evaluated and its loss is selected for in tumoral conditions (5, 64), we here show that the stress imposed by loss of attachment to the cancer cell requires instead the metabolic activity of PML for survival. In further support of our hypothesis, expression of PML has been shown to support luminal filling in a 3D model of breast cancer in vitro. In glandular cancers, tumor cells are displaced from their normal matrix niches in the early stages of tumorigenesis when they proliferate into the lumen of hollow glan-

dular structures. Filling of the luminal space is one of the hallmarks of early tumorigenesis; hence, it is believed that protooncogenic events such as ERBB2 overcome the metabolic stress and cell death response induced by loss of attachment through the recovery of metabolic homeostasis (10). The fact that PML, an established tumor suppressor, could phenocopy ERBB2 in these experimental settings is itself unexpected and noteworthy. It should be noted, however, that the enhanced metabolic and energetic activity observed in PML-overexpressing cells undergoing metabolic stress could also bestow cell fitness and survival to cancer cells in other settings.

Importantly, our analysis in human breast cancer specimens provides firm evidence in line with this unanticipated role of PML in breast cancer biology. First, we have demonstrated that overexpression of PML is predominant in the breast cancer subtypes TNBC and basal (Figure 6, Supplemental Figure 5, and ref. 65). We also have found that the upregulation of PML in tumor cells correlates with that observed in mRNA samples. However, it is worth noting that other factors could mediate the upregulation of PML, including oxidative stress (66) and aberrant PML translation (58).

In addition, PML overexpression correlates with mutation of *Tp53*. This finding is particularly intriguing, since it demonstrates that in these tumors, PML overexpression is disentangled from its ability to activate the p53 tumor-suppressive program (5, 64). Thus, uncoupling of the p53-dependent tumor-suppressive activities of PML from its tumor-promoting metabolic role may provide the selective advantage described herein.

Finally, PML expression is associated with reduced disease-free survival and also with a signature of poor prognosis (60). The assessment of PML status could represent a useful prognostic marker in breast cancer. Immunohistochemical assessment of PML status represents an inexpensive and precise methodology that has been successfully and routinely established as a diagnostic approach in acute promyelocytic leukemia (67) and hence could be easily translated to other tumor types. Moreover, on the basis of our data, PML targeting could offer a new therapeutic modality in breast cancer. PML can be pharmacologically targeted through the use of ATO, a well-tolerated drug that has been extensively employed for the treatment of leukemia (68) and is highly effective in promoting PML degradation at low doses. On the basis of our findings, we hypothesize that targeting PML and FAO in advanced TNBC with combinations of ATO and targeted therapies might represent a novel therapeutic avenue in the treatment of this deadly disease.

Methods

Cell culture. All MEFs were prepared from embryos at day 13.5 of development (E13.5). Early passage (P2–P5) MEFs or RasE1A-transformed MEFs were used. ATO (Sigma-Aldrich) was prepared at a concentration of 0.1 mol l^{-1} in NaOH and subsequently diluted to 1 mmol l^{-1} in PBS. Palmitate, carnitine, etomoxir, L165,041 (Sigma-Aldrich), GW6471 (Tocris), and Wy14643 (Enzo Life Sciences) were prepared in DMSO (palmitate, L165,041, Wy14643) and H_2O (carnitine and etomoxir). Transfections were performed using Effectene following the manufacturers' instructions. All PML overexpression experiments were carried out by transfecting or transducing a PML-IV isoform. Retroviral infections were performed as previously described (69). Primary hepatocytes were isolated using a 2-step perfusion protocol based on a previous method (70).

Microarray and bioinformatic analysis. *Pml*-WT and -KO male 129sv mice were fed a purified control diet (TD.08806; Harlan) and liver tissue was harvested at 32–35 weeks of age after a 6- to 8-hour fasting (9 am to 3–5 pm) in order to avoid effects of immediate food intake. Total RNA from liver tissue was extracted using Trizol (Invitrogen) and followed by RNA purification and DNA digestion using the RNeasy Kit (QIAGEN). Linear amplification of RNA was performed with the Ovation Kit (Nugen), and labelled cDNA was applied to oligonucleotide microarrays (Affymetrix). Affymetrix DAT files were processed using the Affymetrix Gene Chip Operating System (GCOS) to create .CEL files. The quality of scanned array images was determined on the basis of background values, percentage of present calls, scaling factors, and 3′–5′ ratio of β-actin and GAPDH using the Bioconductor R Packages (71) The high-quality arrays were normalized by a robust multi-chip analysis (RMA) package (Bioconductor Telease 2.0) with PM-only models. The differentially expressed genes among the 2 classes were defined using a random-variance *t* test. The random-variance *t* test is an improvement over the standard separate *t* test, as it permits sharing information among genes about within-class variation without assuming that all genes have the same variance (72). Genes were considered statistically significant if their *P* values were less than 0.05. *P* values for significance were computed based on 10,000 random permutations at a nominal significance level of each univariate test of 0.05. The microarray data are publicly available (GEO GSE39220).

GO enrichment analysis. The likelihood of overrepresentation of GO categories in the differentially expressed genes relative to the background of all mouse genes was calculated using Database for Annotation, Visualization and Integrated Discovery (DAVID). DAVID is an online implementation of the EASE software that produces the list of overrepresented categories using jackknife iterative resampling of Fisher's exact test probabilities. The GO ontology categories with a *P* value of less than 0.05 have significant overrepresentation of differentially expressed genes (73, 74).

Promoter analysis. Promoter analysis was performed using the online tool ExPlain 3.0 (http://explain.biobase-international.com/) for detection of overrepresented transcription factor binding sites. For the analysis, we selected regions from 1,000-bp upstream to 100-bp downstream of the transcription start site of each gene (Yes set) and a random set of promoters obtained from mouse housekeeping genes (No set). The entire vertebrate nonredundant set of transcription factors matrix from the TRANSFAC database was used for scanning potential binding sites (75).

GSEA analysis. GSEA was performed using the GSEA-R, a Bioconductor implementation of GSEA from Broad Institute (61). GSEA analysis was performed either using curated gene sets from the molecular signature database from the Broad Institute or by developing gene sets using a standard approach. Analysis was run with 1,000 permutations and a classic statistic. Normalized enrichment score (NES) and nominal *P* value were measured.

Loss of attachment and 3D basement membrane cultures. For the measure of ATP in detached cells (normalized by protein content), the ATP determination kit (Invitrogen) was used. Cells were plated in 6-well poly-HEMA–coated plates at a density of 400,000 cells per well. After 24 hours, cells were lysed in 1% NP40 (plus protease inhibitors) and lysates were normalized by protein content using BCA Protein Assay (Pierce Biotechnology). Lysates were then tested for ATP levels according to the manufacturer's protocol. To measure caspase activity, the caspase-GLO assay (Promega) was used according to the manufacturer's instructions. To generate acini in 3D culture, cells were grown in reconstituted basement membrane (Matrigel) as described previously and according to the protocol from the Brugge laboratory (http://brugge.med.harvard.edu; ref. 76). Immunofluorescence of acini was performed as described previously (76). The following primary antibodies were used for immunofluorescence: cleaved caspase-3 (9661; Cell Signaling Technology) and laminin-5 (mab19562; Millipore). DAPI (Sigma-Aldrich) was used to counter-stain nuclei.

Quantitative real-time PCR. Total RNA was extracted from cells using Trizol (Invitrogen). For liver tissue analysis, total RNA was extracted using Trizol (Invitrogen) and followed by RNA purification and DNA

digestion using RNeasy Kit (QIAGEN). cDNA was obtained with Transcriptor (Roche). TaqMan probes were obtained from Applied Biosystems and selected to avoid detection of genomic DNA. Amplifications were run in a 7900 and a VIIA7 Real-Time PCR System (Applied Biosystems). Each value was adjusted by using *Glucuronidase B* (cells), β-actin (human tissue samples), or *36b4/Rplp0* (liver tissue) levels as reference.

Western blotting, immunoprecipitation, and immunofluorescence. Cells were harvested and protein was extracted as previously described (77). Acetylation experiments were performed as previously described (39). Briefly, cells were transfected with pcDNA-Flag-PGC1A and Flag-GCN5 in a 4:1 ratio, with pLNCX or pLNCX-(HA)PMLIV, as indicated. After 24–48 hours, cells were lysed in 40 mM Tris (pH 7.6), 150 mM NaCl, 1 mM EDTA, 1 mM $MgCl_2$, 1% Triton X-100, 1 mM sodium ortho-vanadate (Na3VO4), 1 mM NaF, 1 mM β-glycerophosphate, 14 mM nicotinamide, 400 nM trichostatin, and protease inhibitor cocktail (Hoffmann–La Roche), cleared by centrifugation, and subjected to immunoprecipitation with Flag-conjugated beads (Sigma-Aldrich) (in the same buffer with 0.1% Triton X-100). After 2 to 3 hours, beads were washed, resuspended in Laemmli Loading Buffer (Boston Bioproducts), and boiled, and the supernatant was subjected to SDS-PAGE. Proteins were detected using a rabbit polyclonal anti-PML antibody (Bethyl), anti-PGC1A antibody (H-300, Santa Cruz Biotechnology Inc.), anti–acetyl lysine (Cell Signaling), HSP90 (Cell Signaling), and anti–β-actin mAb (Sigma-Aldrich). The complete unedited blots for all Western blotting images in the main and supplemental figures are shown in the supplemental material. For immunofluorescence experiments, cells were fixed in 4% paraformaldehyde (15 minutes), permeabilized in 0.1% Triton X-100 (5 minutes), and incubated with primary antibodies overnight (anti-HA mouse [Covance], anti-HA rabbit [Sigma-Aldrich], anti-Flag M2 [Sigma-Aldrich], anti-PML [Bethyl]) after blocking in 10% goat serum (1 hour). For detection, cell slides were incubated with conjugated secondary antibodies anti-mouse A488, anti-rabbit A594, anti-mouse A647, and/or anti-rabbit A546 (Invitrogen). Finally, slides were washed, incubated with DAPI, and mounted in MOWIOL (Sigma-Aldrich). Confocal analysis was performed in a Zeiss LSM 510 Meta Confocal Microscope (Carl Zeiss).

PPAR activity assay. HEK293T cells plated in 48-well plates were transfected with pLNCX or pLNCX-(HA)PMLIV in combination with 3XPPRE-luciferase reporter, PPARα, RXRα, and β-galactosidase. The following day, cells were treated with WY14643 or DMSO in the presence of medium supplemented with 10% FBS. After 16 hours of treatment, cells were lysed and lysates assayed for luciferase activity and β-galactosidase activity (78). Notably, WY14643 treatment consistently resulted in a 2-fold increase in luciferase reporter activity. The extent of luciferase reporter activation in these conditions could be due to the presence of serum in the experimental design.

Mouse analysis. For HFD analysis, 3-month-old *Pml*-WT and -KO 129Sv male mice were randomly assigned to the experimental groups and subjected to a control diet (TD.08806; Harlan Teklad) or to a HFD (TD.06414; Harlan Teklad). Mice were monitored for 20 weeks and afterwards subjected to analysis of body mass by EchoMRI, glucose tolerance test (GTT), and analysis food intake and activity (measured in metabolic chambers). For tissue and serum harvesting, mice were deprived of food for 6–8 hours in daytime (9 am to 3–5 pm) in order to avoid effects due to immediate food intake. Serum leptin was measured by ELISA (Mouse Leptin ELISA Kit; Crystal Chem Inc.). For GTT, mice were fasted from 8 am to 4 pm and placed in wood-bedding cages; then glucose was injected at 2 g/kg and blood glucose dynamics were measured with a glycosometer from the tail vein. For Lep^{Ob} mouse analysis, *Pml-*Lep^{Ob} double-mutant mice were weaned at 4 weeks of age, genotyped, and monitored for body weight and body mass composition at the indicated time points.

Patient samples and IHC. Tumor and patient characteristics, tissue microarray construction, and gene expression profiles were reported previously (53, 79, 80). The IHC detection was performed on 4-μm sections with the MOM kit from Vector Laboratories. Rabbit polyclonal PML antibody (Santa Cruz Biotechnology Inc.) was used in 1:500 dilution; mouse Pml mAb (MAB3738; Chemicon) was used in 1:500 dilution. IHC detection was performed with the ABC Kit from Vector Laboratories. All IHC sections were evaluated by A.L. Richardson, and the histological diagnosis was based on established criteria.

FAO. Cells were incubated overnight in culture medium containing 100 μM palmitate (C16:0) and 1 mM carnitine. In the final 2 hours of incubation, cells were pulsed for 2 hours with 1.7 μCi [9,10(n)-^{3}H]palmitic acid (GE Healthcare) in the presence or absence of etomoxir (100 μM; Sigma-Aldrich), and the medium was collected to analyze the released ^3H_2O formed during cellular oxidation of [^{3}H]palmitate (39, 81). Briefly, medium was TCA precipitated, and supernatants were neutralized with NaOH and loaded onto ion exchange columns packed with DOWEX 1X2-400 resin (Sigma-Aldrich). The radioactive product was eluted with water and quantitated by liquid scintillation counting. Oxidation of [^{3}H]palmitate was normalized to protein content using Bio-Rad DC Protein Assay. Etomoxir, a specific inhibitor of CPT1a, was used to specifically inhibit mitochondrial FAO. In MCF10A cells, FAO was measured as previously described (10).

Statistics. Statistical significance was evaluated by using Student's 2-tailed *t* test unless otherwise specified. A *P* value of less than 0.05 was considered statistically significant.

Study approval. The animal protocol was reviewed and approved by the Beth Israel Deaconess Medical Center Institute Animal Care and Use Committee (IACUC). The human specimen analysis complied with all ethics requirements and was approved by the Dana-Farber/Harvard Cancer Center Institutional Review Board (tissue banking protocol 93-085).

Acknowledgments

We thank P. Hemmerich and I. Kitabayashi for sharing valuable reagents. We thank all members of the Pandolfi lab, in particular, R.M. Hobbs, D. Sciaranghella, M.S. Song, and L. Salmena as well as J. Brugge, A. Grassian, and M. Serrano for advice and technical support. This work was supported by NIH grants to P.P. Pandolfi and partially supported by the NCI Harvard SPORE in breast cancer (2P50 CA089393) and the Breast Cancer Research Foundation (to A.L. Richardson). The work of A. Carracedo was supported by EMBO, the Ramón y Cajal award (Spanish Ministry of Education), the ISCIII (PI10/01484), the Marie Curie IRG grant (277043), and the Basque Government of Education (PI2012-03).

Received for publication November 29, 2011, and accepted in revised form July 5, 2012.

Address correspondence to: Pier P. Pandolfi, 330 Brookline Avenue, CLS-401, Boston, Massachusetts 02215, USA. Phone: 617.735.2121; Fax: 617.735.2120; E-mail: ppandolf@bidmc.harvard.edu.

1. Vander Heiden MG, Cantley LC, Thompson CB. Understanding the Warburg effect: the metabolic requirements of cell proliferation. *Science*. 2009; 324(5930):1029–1033.
2. Koppenol WH, Bounds PL, Dang CV. Otto Warburg's contributions to current concepts of cancer metabolism. *Cancer*. 2011;11(5):325–337.
3. Locasale JW, Cantley LC. Metabolic flux and the regulation of Mammalian cell growth. *Cell Metab*. 2011;14(4):443–451.
4. Hanahan D, Weinberg RA. Hallmarks of cancer: the next generation. *Cell*. 2011;144(5):646–674.
5. Bernardi R, Pandolfi PP. Structure, dynamics and functions of promyelocytic leukaemia nuclear bodies. *Nat Rev Mol Cell Biol*. 2007;8(12):1006–1016.
6. Zhong S, Hu P, Ye TZ, Stan R, Ellis NA, Pandolfi PP. A role for PML and the nuclear body in genomic stability. *Oncogene*. 1999;18(56):7941–7947.

7. Shen TH, Lin HK, Scaglioni PP, Yung TM, Pandolfi PP. The mechanisms of PML-nuclear body formation. *Mol Cell*. 2006;24(3):331–339.
8. Lang M, et al. Three-dimensional organization of promyelocytic leukemia nuclear bodies. *J Cell Sci*. 2010; 123(pt 3):392–400.
9. Carracedo A, Ito K, Pandolfi PP. The nuclear bodies inside out: PML conquers the cytoplasm. *Curr Opin Cell Biol*. 2011;23(3):360–366.
10. Schafer ZT, et al. Antioxidant and oncogene rescue of metabolic defects caused by loss of matrix attachment. *Nature*. 2009;461(7260):109–113.
11. Samudio I, Fiegl M, Andreeff M. Mitochondrial uncoupling and the Warburg effect: molecular basis for the reprogramming of cancer cell metabolism. *Cancer Res*. 2009;69(6):2163–2166.
12. Zuagg K, et al. Carnitine palmitoyltransferase 1C promotes cell survival and tumor growth under conditions of metabolic stress. *Genes Dev*. 2011; 25(10)1041–1051.
13. Samudio I, et al. Pharmacologic inhibition of fatty acid oxidation sensitizes human leukemia cells to apoptosis induction. *J Clin Invest*. 2010; 120(1):142–156.
14. Tatham MH, et al. RNF4 is a poly-SUMO-specific E3 ubiquitin ligase required for arsenic-induced PML degradation. *Nat Cell Biol*. 2008;10(5):538–546.
15. Lallemand-Breitenbach V, et al. Arsenic degrades PML or PML-RARalpha through a SUMO-triggered RNF4/ubiquitin-mediated pathway. *Nat Cell Biol*. 2008;10(5):547–555.
16. Fei M, et al. Arsenic trioxide-induced growth arrest of human hepatocellular carcinoma cells involving FOXO3a expression and localization. *Med Oncol*. 2009;26(2):178–185.
17. Siu KP, Chan JY, Fung KP. Effect of arsenic trioxide on human hepatocellular carcinoma HepG2 cells: inhibition of proliferation and induction of apoptosis. *Life Sci*. 2002;71(3):275–285.
18. Ji H, Friedman MI. Reduced hepatocyte fatty acid oxidation in outbred rats prescreened for susceptibility to diet-induced obesity. *Int J Obes (Lond)*. 2008; 32(8):1331–1334.
19. Ji H, Friedman MI. Reduced capacity for fatty acid oxidation in rats with inherited susceptibility to diet-induced obesity. *Metabolism*. 2007;56(8):1124–1130.
20. Orellana-Gavalda JM, et al. Molecular therapy for obesity and diabetes based on a long-term increase in hepatic fatty-acid oxidation. *Hepatology*. 2011;53(3):821–832.
21. Zhang D, et al. Resistance to high-fat diet-induced obesity and insulin resistance in mice with very long-chain acyl-CoA dehydrogenase deficiency. *Cell Metab*. 2010;11(5):402–411.
22. Harrington WW, et al. The effect of PPARalpha, PPARdelta, PPARgamma, and PPARpan agonists on body weight, body mass, and serum lipid profiles in diet-induced obese AKR/J mice. *PPAR Res*. 2007; 2007:97125.
23. Feige JN, et al. Specific SIRT1 activation mimics low energy levels and protects against diet-induced metabolic disorders by enhancing fat oxidation. *Cell Metab*. 2008;8(5):347–358.
24. Pfluger PT, Herranz D, Velasco-Miguel S, Serrano M, Tschop MH. Sirt1 protects against high-fat diet-induced metabolic damage. *Proc Natl Acad Sci U S A*. 2008;105(28):9793–9798.
25. Purushotham A, Schug TT, Xu Q, Surapureddi S, Guo X, Li X. Hepatocyte-specific deletion of SIRT1 alters fatty acid metabolism and results in hepatic steatosis and inflammation. *Cell Metab*. 2009; 9(4):327–338.
26. Kim MK, et al. Promyelocytic leukemia inhibits adipogenesis, and loss of promyelocytic leukemia results in fat accumulation in mice. *Am J Physiol Endocrinol Metab*. 2011;301(6):E1130–E1142.
27. Lindstrom P. The physiology of obese-hyperglycemic mice [ob/ob mice]. *ScientificWorldJournal*. 2007;7:666–685.
28. Nguyen P, et al. Liver lipid metabolism. *J Anim Physiol Anim Nutr (Berl)*. 2008;92(3):272–283.
29. Guillou H, Martin PG, Pineau T. Transcriptional regulation of hepatic fatty acid metabolism. *Subcell Biochem*. 2008;49:3–47.
30. Kiec-Wilk B, Dembinska-Kiec A, Olszanecka A, Bodzioch M, Kawecka-Jaszcz K. The selected pathophysiological aspects of PPARs activation. *J Physiol Pharmacol*. 2005;56(2):149–162.
31. Peters JM, Gonzalez FJ. Sorting out the functional role(s) of peroxisome proliferator-activated receptor-beta/delta (PPARbeta/delta) in cell proliferation and cancer. *Biochim Biophys Acta*. 2009; 1796(2):230–241.
32. Rakhshandehroo M, et al. Comprehensive analysis of PPARalpha-dependent regulation of hepatic lipid metabolism by expression profiling. *PPAR Res*. 2007;2007:26839.
33. Degenhardt T, et al. Three members of the human pyruvate dehydrogenase kinase gene family are direct targets of the peroxisome proliferator-activated receptor beta/delta. *J Mol Biol*. 2007; 372(2):341–355.
34. Sugden MC, Holness MJ. Mechanisms underlying regulation of the expression and activities of the mammalian pyruvate dehydrogenase kinases. *Arch Physiol Biochem*. 2006;112(3):139–149.
35. Kitamura YI, et al. FoxO1 protects against pancreatic beta cell failure through NeuroD and MafA induction. *Cell Metab*. 2005;2(3):153–163.
36. Puigserver P, Spiegelman BM. Peroxisome proliferator-activated receptor-gamma coactivator 1 alpha (PGC-1 alpha): transcriptional coactivator and metabolic regulator. *Endocr Rev*. 2003;24(1):78–90.
37. Sugden MC, Caton PW, Holness MJ. PPAR control: it's SIRTainly as easy as PGC. *J Endocrinol*. 2010; 204(2):93–104.
38. Puigserver P. Tissue-specific regulation of metabolic pathways through the transcriptional coactivator PGC1-alpha. *Int J Obes (Lond)*. 2005;1:S5–9.
39. Gerhart-Hines Z, et al. Metabolic control of muscle mitochondrial function and fatty acid oxidation through SIRT1/PGC-1alpha. *EMBO J*. 2007; 26(7):1913–1923.
40. Estall JL, et al. Sensitivity of lipid metabolism and insulin signaling to genetic alterations in hepatic peroxisome proliferator-activated receptor-gamma coactivator-1alpha expression. *Diabetes*. 2009; 58(7):1499–1508.
41. Finck BN, et al. Lipin 1 is an inducible amplifier of the hepatic PGC-1alpha/PPARalpha regulatory pathway. *Cell Metab*. 2006;4(3):199–210.
42. Dominy JE Jr, Lee Y, Gerhart-Hines Z, Puigserver P. Nutrient-dependent regulation of PGC-1alpha's acetylation state and metabolic function through the enzymatic activities of Sirt1/GCN5. *Biochim Biophys Acta*. 2010;1804(8):1676–1683.
43. Lerin C, Rodgers JT, Kalume DE, Kim SH, Pandey A, Puigserver P. GCN5 acetyltransferase complex controls glucose metabolism through transcriptional repression of PGC-1alpha. *Cell Metab*. 2006; 3(6):429–438.
44. Rodgers JT, Lerin C, Gerhart-Hines Z, Puigserver P. Metabolic adaptations through the PGC-1 alpha and SIRT1 pathways. *FEBS Lett*. 2008;582(1):46–53.
45. Rodgers JT, Lerin C, Haas W, Gygi SP, Spiegelman BM, Puigserver P. Nutrient control of glucose homeostasis through a complex of PGC-1alpha and SIRT1. *Nature*. 2005;434(7029):113–118.
46. Gerhart-Hines Z, et al. The cAMP/PKA pathway rapidly activates SIRT1 to promote fatty acid oxidation independently of changes in NAD(+). *Mol Cell*. 2012;44(6):851–863.
47. Pighetti GM, et al. Therapeutic treatment of DMBA-induced mammary tumors with PPAR ligands. *Anticancer Res*. 2001;21(2A):825–829.
48. Suchanek KM, et al. Peroxisome proliferator-activated receptor alpha in the human breast cancer cell lines MCF-7 and MDA-MB-231. *Mol Carcinog*. 2002; 34(4):165–171.
49. Xu HE, et al. Structural basis for antagonist-mediated recruitment of nuclear co-repressors by PPARalpha. *Nature*. 2002;415(6873):813–817.
50. Shaw KR, Wrobel CN, Brugge JS. Use of three-dimensional basement membrane cultures to model oncogene-induced changes in mammary epithelial morphogenesis. *J Mammary Gland Biol Neoplasia*. 2004;9(4):297–310.
51. Gurrieri C, et al. Loss of the tumor suppressor PML in human cancers of multiple histologic origins. *J Natl Cancer Inst*. 2004;96(4):269–279.
52. Desmedt C, et al. Biological processes associated with breast cancer clinical outcome depend on the molecular subtypes. *Clin Cancer Res*. 2008; 14(16):5158–5165.
53. Matros E, Wang ZC, Lodeiro G, Miron A, Iglehart JD, Richardson AL. BRCA1 promoter methylation in sporadic breast tumors: relationship to gene expression profiles. *Breast Cancer Res Treat*. 2005;91(2):179–186.
54. Wang ZC, et al. Loss of heterozygosity and its correlation with expression profiles in subclasses of invasive breast cancers. *Cancer Res*. 2004;64(1):64–71.
55. Thor AD, et al. Accumulation of p53 tumor suppressor gene protein: an independent marker of prognosis in breast cancers. *J Natl Cancer Inst*. 1992; 84(11):845–855.
56. Sorlie T, et al. Gene expression patterns of breast carcinomas distinguish tumor subclasses with clinical implications. *Proc Natl Acad Sci U S A*. 2001; 98(19):10869–10874.
57. Soong R, et al. Concordance between p53 protein overexpression and gene mutation in a large series of common human carcinomas. *Hum Pathol*. 1996; 27(10):1050–1055.
58. Scaglioni PP, et al. Translation-dependent mechanisms lead to PML upregulation and mediate oncogenic K-RAS-induced cellular senescence. *EMBO Mol Med*. 2012;4(7):594–602.
59. Huber KE, Carey LA, Wazer DE. Breast cancer molecular subtypes in patients with locally advanced disease: impact on prognosis, patterns of recurrence, and response to therapy. *Semin Radiat Oncol*. 2009;19(4):204–210.
60. van 't Veer LJ, et al. Gene expression profiling predicts clinical outcome of breast cancer. *Nature*. 2002;415(6871):530–536.
61. Subramanian A, et al. Gene set enrichment analysis: a knowledge-based approach for interpreting genome-wide expression profiles. *Proc Natl Acad Sci U S A*. 2005;102(43):15545–15550.
62. Ito K, et al. A PML-PPARδ pathway for fatty acid oxidation regulates hematopoietic stem cell maintenance. *Nat Med*. 2012. In press.
63. Ito K, et al. PML targeting eradicates quiescent leukaemia-initiating cells. *Nature*. 2008; 453(7198):1072–1078.
64. Bernardi R, Papa A, Pandolfi PP. Regulation of apoptosis by PML and the PML-NBs. *Oncogene*. 2008;27(48):6299–6312.
65. Bertucci F, et al. How different are luminal A and basal breast cancers? International journal of cancer. *Int J Cancer*. 2009;124(6):1338–1348.
66. Jeanne M, et al. PML/RARA oxidation and arsenic binding initiate the antileukemia response of As2O3. *Cancer Cell*. 2010;18(1):88–98.
67. Lo-Coco F, Ammatuna E. The biology of acute promyelocytic leukemia and its impact on diagnosis and treatment. *Hematology Am Soc Hematol Educ Program*. 2006:156–161.
68. Emadi A, Gore SD. Arsenic trioxide — An old drug rediscovered. *Blood Rev*. 2010;24(4–5):191–199.
69. Chen Z, et al. Crucial role of p53-dependent cellular senescence in suppression of Pten-deficient tumorigenesis. *Nature*. 2005;436(7051):725–730.
70. Lin J, et al. 2004. Defects in adaptive energy metabo-

lism with CNS-linked hyperactivity in PGC-1alpha null mice. *Cell*. 2004;119(1):121–135.
71. Gentleman RC, et al. Bioconductor: open software development for computational biology and bioinformatics. *Genome Biol*. 2004;5(10):R80.
72. Wright GW, Simon RM. A random variance model for detection of differential gene expression in small microarray experiments. *Bioinformatics*. 2003; 19(18):2448–2455.
73. Huang da W, Sherman BT, Lempicki RA. Systematic and integrative analysis of large gene lists using DAVID bioinformatics resources. *Nat Protoc*. 2009;4(1):44–57.
74. Dennis G, et al. DAVID: Database for Annotation, Visualization, and Integrated Discovery. *Genome Biol*. 2003;4(5):P3.
75. Wingender E, et al. TRANSFAC: an integrated system for gene expression regulation. *Nucleic Acids Res*. 2000;28(1):316–319.
76. Debnath J, Muthuswamy SK, Brugge JS. Morphogenesis and oncogenesis of MCF-10A mammary epithelial acini grown in three-dimensional basement membrane cultures. *Methods*. 2003;30(3):256–268.
77. Alimonti A, et al. A novel type of cellular senescence that can be enhanced in mouse models and human tumor xenografts to suppress prostate tumorigenesis. *J Clin Invest*. 2010;120(3):681–693.
78. Houten SM, et al. Pyruvate dehydrogenase kinase 4 expression is synergistically induced by AMP-activated protein kinase and fatty acids. *Cell Mol Life Sci*. 2009;66(7):1283–1294.
79. Lu X, Wang ZC, Iglehart JD, Zhang X, Richardson AL. Predicting features of breast cancer with gene expression patterns. *Breast Cancer Res Treat*. 2008; 108(2):191–201.
80. Richardson AL, et al. X chromosomal abnormalities in basal-like human breast cancer. *Cancer Cell*. 2006;9(2):121–132.
81. Deberardinis RJ, Lum JJ, Thompson CB. Phosphatidylinositol 3-kinase-dependent modulation of carnitine palmitoyltransferase 1A expression regulates lipid metabolism during hematopoietic cell growth. *J Biol Chem*. 2006;281(49):37372–37380.
82. Elston CW, Ellis IO. Pathological prognostic factors in breast cancer. *Histopathology*. 1991;19(5):403–410.